Microchimica Acta (2021) 188:173
https://doi.org/10.1007/s00604-021-04824-y

ORIGINAL PAPER

A sensitive and label-free electrochemical microRNA biosensor based on Polyamidoamine Dendrimer functionalized Polypyrrole nanowires hybrid

Dongwei Wang[1] · Jiasheng Wang[1]

Received: 14 August 2020 / Accepted: 6 April 2021

Abstract

The potential of functionalized polypyrrole nanowires (PPyNWs) are demonstrated as a platform for lable-free miRNA detection using electrochemical impedance spectroscopy (EIS). MicroRNAs (miRNAs) detection methods and sensors are mainly challenged by very low concentrations in physiological samples and high similarity among family members. Herein, a sensitive and selective miRNA biosensor was constructed based on electrochemically synthesized PPyNWs, which were functionalized with polyamidoamine dendrimer (PAMAM) by an electro-oxidation method. The prepared PPyNWs/PAMAM hybrid combines the excellent electrical conductivity of conducting polymer PPyNWs with high surface to volume ratio of PAMAM. DNA probes were immobilized onto the PPyNWs/PAMAM hybrid for the construction of the miRNA biosensor. Using the sensitive EIS technique to monitor DNA/miRNA hybridization, the developed biosensor demonstrated excellent sensing performances, such as wide linear range (10^{-14} M-10^{-8} M) and low detection limit (0.34×10^{-14} M). Even more encouraging, the response sensitivity of the biosensor was 3.12 times higher than that of the bulk PPy-modified sensor, which proved that the microstructure of the PPy nanowires array can greatly improve the performance of the biosensor.

Keywords Conducting polymer · Polypyrrole nanowires · Polyamidoamine dendrimer · microRNA · Biosensor

Introduction

The study of microRNAs (miRNAs) has attracted more and more attention in the life sciences because increasing evidence has demonstrated that miRNAs play important role in the onset and progression of most human malignancies [1]. Aberrant expressions of miRNAs (higher or lower concentrations) are highly associated with various cancers. For instance, miRNA21 has been found to be expressed at higher level in gastric cancer patients' blood serum; while miRNA155 are under-expressed in the cancer stages of breast cancer [2–4]. Accordingly, miRNA quantitative profiles represent an attractive biomarker for early cancer diagnosis, assessing prognosis, and monitoring therapeutic efficacy [5]. For the quantification of miRNAs, their intrinsic characteristics, such as small size (19–23 nucleotides), high sequence similarity and wide dynamic range (from aM to nM), bring major challenges to the most commonly used methods [2, 6]. Biofouling of solid carriers, low throughput, difficulty in amplification or miniaturization, time-consuming and laborious preparation and separation procedures, and complex and expensive analysis are all problems that limit the application of clinical diagnosis [6]. In recent years, electrochemical biosensors have attracted more attention because of their great advantages such as low cost, portable instrumentation, convenient operation, high sensitivity and good selectivity [7–9].

Nanomaterial and functionalized nanomaterial have been introduced into biosensors to improve the sensitivity by speeding up the electron transfer and increasing the electroactive surface area of electrodes. Polypyrrole (PPy), as a promising one in the conducting polymer family, is playing an important role in the development of high-performance electrochemical biosensors because of its good stability, ordinary preparation, benign conductivity, excellent biocompatibility and versatility [10–12]. In addition to such versatile and beneficial performances of conducting PPy, the large surface area and highly aligned architecture of PPy nanowires array (PPyNWs) make them ideal for the construction of nanoelectronic devices and sensors [13, 14]. For instance, well-ordered PPyNWs arrays on surfaces of carbon

✉ Jiasheng Wang
jiasheng0813@163.com

[1] Qingdao Agricultural University, Qingdao 266109, China

Published online: 23 April 2021

fibers have been prepared for pseudocapacitor electrodes with high performance. The superior performance has been proved mainly due to highly aligned nanoarchitecture arrays, which can create a novel way to speed up Faradaic reactions for charge storage and solve "dead volume" problems [15]. Functionalized PPy nanomaterials with high surface area, enhanced electron transfer ability and hydrophilic character have been a promising platform for electrochemical biosesnors and can be used for the detection of DNA, microRNA and autocrine motility factor (phosphoglucose isomerase) [16–20].

The fourth generation poly(amidoamine) polymers (PAMAM), one particular class of dendrimers, has been successfully used for the fabrication of (bio)sensors because of the nanoscopic spherical structure and good biocompatibility [21]. PAMAM possesses abundant amine groups with high density in the branched chains, which are easily functionalized by other substances [22]. PAMAM dendrimers modified with MWCNTs have been successfully applied to fabricate an electrochemical aptamer biosensor of human cellular prions PrPC. These results have demonstrated that the used PAMAM can improve high surface coverage of probe DNA and the dendrimer modified biosensor can detect proteins PrPC in pM concentration level [23]. Electrochemical modification of PPy film by amine oxidation of PAMAM has been prepared and has been used for application of DNA biosensor [24]. Thus, integration of PPy with PAMAM by the copolymerization or covalently attachment can greatly add the number of functional biomolecules, thus effectively improving the sensitivity of the assay [25]. However, the grafting of PAMAM dendrimer onto PPyNWs has rarely been explored. The ultrasensitive and selective miRNA detection in real biological samples remains a challenge.

In this work, based on the PPyNWs/PAMAM hybrid, a reagentless electrochemical miRNA biosensor was developed. MiRNA24 was used as model target in this work. PAMAM has been electrodeposited onto un-functionalized PPyNWs surface through electrochemical oxidation of PAMAM amine groups. The covalent grafting method of PAMAM and PPyNWs has many advantages, such as short time, simple operation and no need to process the pyrrole monomer in advance [24]. A huge amount of amine of PPyNWs/PAMAM allows the immobilizations of large amounts of DNA probes. Electrochemical impedance spectroscopy (EIS) technique was adopted to monitor the sensing performance, and it was found that the biosensor demonstrated satisfying biosensing performance for the detection of miRNA.

Experimental

Reagents and apparatus

Pyrrole, N-hydroxysuccinimde (NHS), 1-ethyl-3-(3-dimethylaminopropyl) carbodiimide (EDC), p-toluenesulfonate Sodium (TsONa), $K_4Fe(CN)_6 \cdot H_2O$, $K_3Fe(CN)_6$, NaH_2PO_4, $Na_2HPO_4 \cdot 12H_2O$ and KCl were purchased from Aladdin Regent (Shanghai, China). PAMAM (G3) of third generation was purchased from Weihai Chenyuan Molecular New Material Co., Ltd. (Weihai, China). Human hemoglobin (Hb), lysozyme (LZ), human serum albumin (HSA), DNA probes, miRNA24, miRNA21 and the related mismatch miRNA24 were obtained from Shanghai Shenggong co. LTD (Shanghai, China). The synthetic 5′-carboxyl group terminated DNA capture probes (C1), miRNA24 (T2), single-based mismatch miRNA24 (M1), three-based mismatch miRNA24 (M2) and miRNA21 (M3) are shown in Table S1.

Apparatus

A CHI660E Electrochemical Workstation (Shanghai CH Instrument Co., China) was used to carry out all electrochemical tests. A traditional three-electrode system was employed with a modified glassy carbon electrode (GCE, 3.0 mm, the working electrode), a platinum wire (the counter electrode) and a saturated calomel electrode (SCE, the reference electrode). JEOL JSM-7500F (Hitachi High Technology Co., Ltd., Japan) was employed to perform scanning electron microscope (SEM) experiments. Thermo-VG Scientific ESCALAB 250 spectrometer was used to perform X-Ray photoelectron spectroscopy (XPS) analysis.

Preparation of PAMAM/PPyNWs hybrid onto GCE

Before use, GCE was polished using alumina slurries and pretreated in PBS according to the previous report [26]. Neat PPyNWs onto the surface of GCE were successfully prepared by an electrochemical polymerization method. The deposition solution is 5 mL PBS (0.2 M, pH = 6.86) containing 0.15 M pyrrole and 0.1 M TsONa. The constant potential of 0.75 V for 10 min was used to prepare PPyNWs. GCE/PPyNWs was obtained.

As a contrast, bulk PPy was also deposited by the same electrochemical parameters. The electrochemical deposition solution was 5 mL PBS (0.2 M, pH = 6.86) containing 0.15 M pyrrole and 0.1 M $LiClO_4$. This is the only difference from the preparation of PPyNWs. GCE/PPy(bulk) was obtained.

PAMAM dendrimers were grafted onto the surface of PPyNWs (or bulk PPy) through covalent bonding through electrochemical oxidation of amine groups of PAMAM. The mechanism of this reaction is that PAMAM react with polypyrrole membrane by electro-oxidation of the end amines to form free radicals [24]. Electrochemical deposition process was performed in a solution containing 0.05 M PAMAM and 0.1 M $LiClO_4$ by cyclic voltammetry (the potential: 0.0 ~ 1.1 V; 3 cycles; scan rate: 0.10 V s^{-1}). GCE/PPyNWs/PAMAM and GCE/PPy(bulk)/PAMAM were obtained. All

modified electrodes were rinsed three times with PBS and double distilled water respectively.

Preparation of the miRNA biosensor

The preparation procedure of the miRNA biosensor based on PPyNWs/PAMAM is shown in Scheme 1. GCE/PPyNWs/PAMAM was incubated in 1.0 μM C1 solution containing 0.4 M EDC, 0.1 M NHS at room temperature for 1.0 h, to allow C1 covalently fixed to PAMAM of the modified electrode [18]. The obtained sensor was recorded as GCE/PPyNWs/PAMAM/C1. The hybridization reaction was then performed by immersing GCE/PPyNWs/PAMAM/C1 into PBS (0.2 M, pH 7.4) containing T2 for 1.0 h at room temperature. Thus the obtained electrode was defined as GCE/PPyNWs/PAMAM/C1/T2.

Electrochemical impedance spectroscopy (EIS) method was used to record the hybridization reaction between C1 and T2. EIS measurements were performed with current potential of 0.20 V, frequency range of 0.1 ~ 100 KHz, the applied sine wave of 5 mV. All EIS tests were carried out in PBS (0.2 M, pH 7.4) including 0.1 M KCl and 5.0 mM $[Fe(CN)_6]^{3-/4-}$. The EIS value of GCE/PPyNWs/PAMAM/C1 was regarded as the background (R_0). After incubation in different concentration of T2 for 30 min, EIS values were recorded and compared. To test the selectivity of the biosensor, M1, M2 and M3 were used as controls.

Results and discussion

Choice of materials

Conducting polymers (polythiophene, polypyrrole and polyaniline) provide the merits such as cheap and adjustable conductivity. N-substituted PPys have been electrocopolymerized. However, the resulting PPys possessed low conductivity possibly due to a lack of ring planarity in the polymer structure [27]. PPyNWs can be easily prepared without template. Previous scientific studies have proved that ordered PPyNWs can significantly facilitate the mass transport and electron transfer, thus improving sensor performance [19, 20]. For this reason, PPyNWs was selected in this work to fabricate electrochemical electrodes.

Morphologies of PPy nanowires

Well-ordered PPyNWs array was developed by an electrochemical polymerization of pyrrole on the surface of GCE at the constant potential of 0.75 V for 10 min, using TsONa as the soft template. Figure 1 exhibits the morphologies of the PPyNWs array at different magnification. Ordered PPyNWs were vertically aligned on GCE surface (the diameter: 100–400 nm), forming a hierarchical microstructure by conducting polymer nanowire arrays. The larger magnification SEM of PPyNWs shows that the top of the nanowires become thinner and thinner, like cones. The formation mechanism of

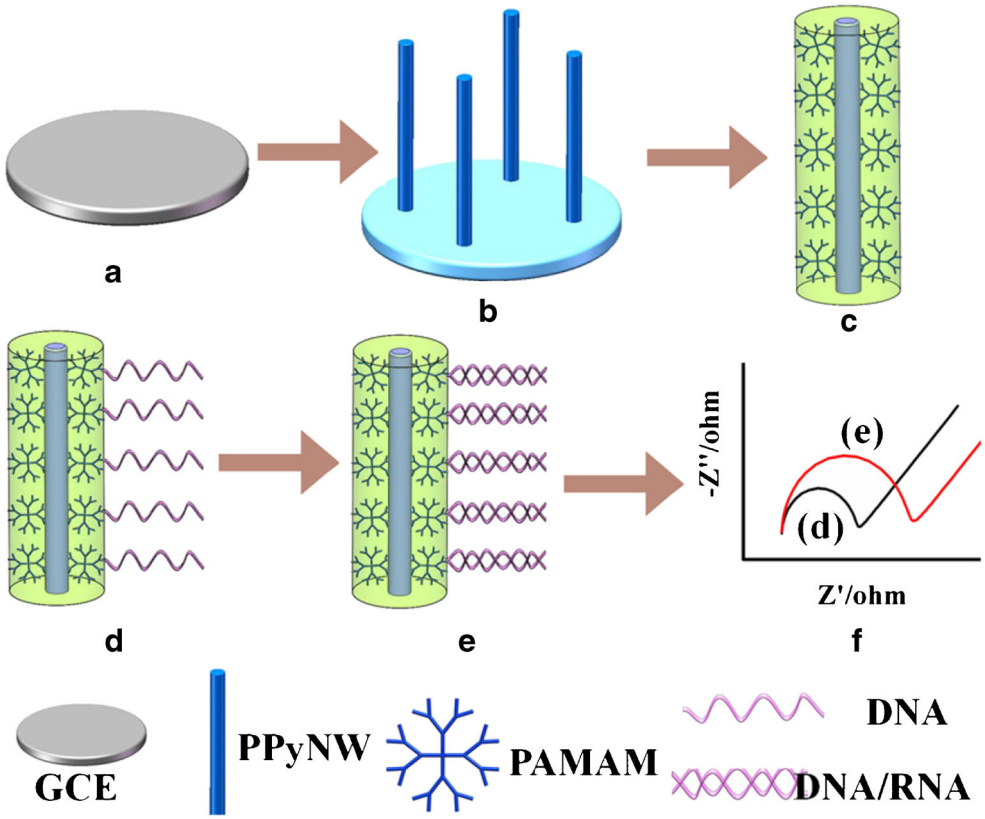

Scheme 1 Schematic diagram of the construction process of GCE/PPyNWs/PAMAM/DNA/RNA. (a) bare GCE, (b) GCE/PPyNWs, (c) GCE/PPyNWs/PAMAM, (d) GCE/PPyNWs/PAMAM/DNA, (e) GCE/PPyNWs/PAMAM/DNA/RNA, (f) EIS plot of electrodes (d) and (e).

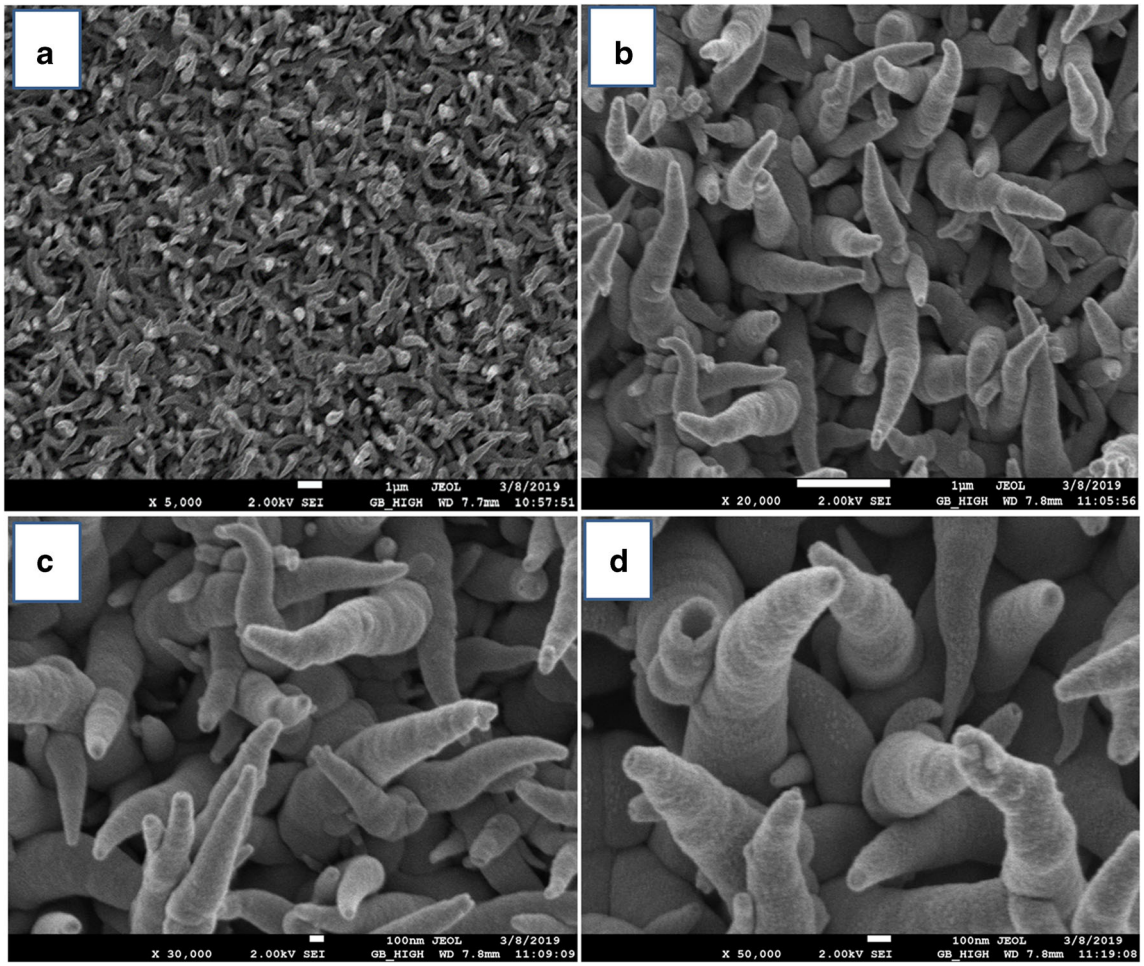

Fig. 1 SEM images of PPyNWs on the surface of GCE at different magnifications

PPyNWs has been reported in the literature [15, 28], which is briefly summarized as the following steps. Pyrrole monomer and TsONa anions gathered and accumulated on the carbon surface, which can act as nucleation sites. The TsONa anions doped PPy oligomers ensured that the PPY grew into a linear shape because of the predominant polymerization at the nuclei tips under the highest electric field. The upward-growing PPyNWs provide convenient ion diffusion paths and fast electron transport channels, which is very important for the high conductivity and sensitivity of electrochemical sensors.

Characterization of PPyNWs/PAMAM

XPS technique were used to verify the successful preparation of PPyNWs/PAMAM nanocomposition. As shown in Fig. 2A and Table S2, C 1 s, N 1 s, S 2p and O 1 s peaks were observed, showing the formation of TsONa doped PPyNWs. After the covalent bonding of PAMAM onto PPyNWs, C 1 s, N 1 s, and S 2p peaks decreased apparently and O 1 s peak increased obviously, together with the new appearance of Cl 2p and Li 1 s peaks, indicating the successful immobilization of PAMAM dendrimers. Fig. S1 shows XPS spectra of carbon (A1, B1) and nitrogen (A2, B2) regions of PPyNWs and PPyNWs/PAMAM. Electrochemical functionalization of PPyNWs with PAMAM resulted into great changes in spectrum of both regions. It has been reported that aliphatic amines can be attached onto the surface of glassy carbon electrode, metal surfaces and CNTs through electrochemical patterning [29–31]. The reaction mechanism is that free radical cation has strong reactivity and can be connected with nucleophilic groups such as aromatic rings, leading to the breaking of double bond C=C and the formation of C-N bond [31, 32]. In this study, PPyNWs were functionalized with PAMAM by amine electrochemical oxidation. The electro-oxidation method used in this work has the advantage of short reaction time and does not require further chemical modification of pyrrole monomer before polymerization.

The static water contact angles of bare GCE, GCE/PPyNWs, GCE/PPyNWs/PAMAM and GCE/PPyNWs/PAMAM/DNA surfaces were measured. As shown in Fig. S2 and Table S2, the contact angle of bare GCE, GCE/PPyNWs and GCE/PPyNWs/PAMAM and GCE/PPyNWs/PAMAM/DNA were 72.2°, 115.4°, 32.4° and 21.9°, respectively. GCE/PPyNWs/PAMAM/DNA surface shows good hydrophilicity [33].

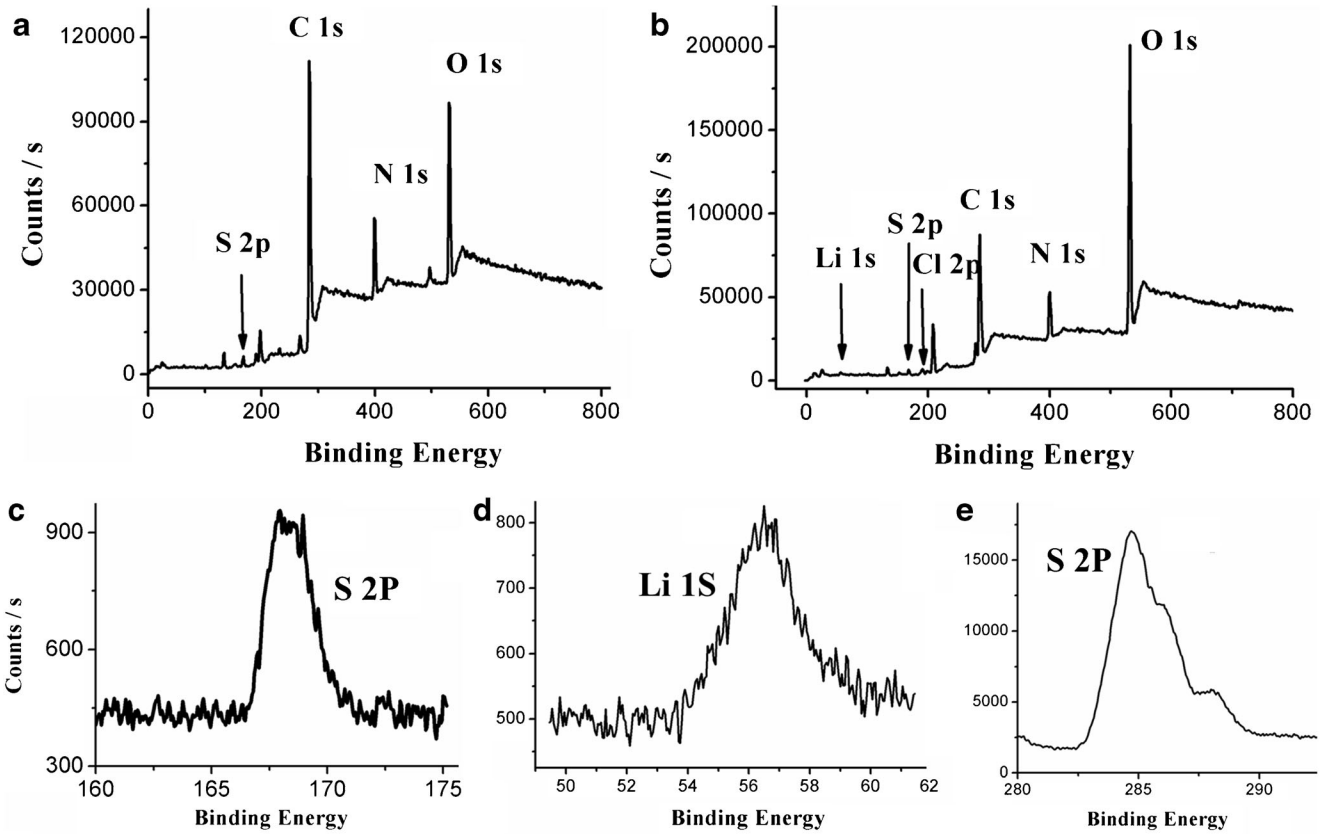

Fig. 2 XPS of PPyNWs (A) and PPyNWs/PAMAM (B). High resolution XPS of single element S 2p (C), Li (D), and Cl (E)

Chronocoulometry was used to estimate the electroactive surface areas of bare GCE, bulk PPy and PPyNWs modified electrodes. According to the Cottrell equation [34],

$$Q(t) = \left(2nFAD^{1/2}\pi^{-1/2}C\right)t^{1/2} + Q_{dl} + Q_{ads}$$

The parameters in the formula are explained as follows: n is the electron number of reaction; Q is the value of the reduction charge; A is the active surface area, C is the concentration, and D is the diffusion coefficient. Figure 3A showed the chronocoulometric plots of three different electrodes. From Fig. 3B, the electoactive surface area of GCE/PPyNWs (curve c, 1.517 cm^2) was estimated, which was 46.0 and 3.13 times larger than that of the bare GCE (curve a, 0.03298 cm^2) and the bulk GCE/PPy (curve b, 0.4844 cm^2), respectively. The experimental results proved that GCE/PPyNWs can provide larger eletroactive surface areas, which is beneficial for the establishment of high-performance sensing platform. In addition, we have completed the experiment of nitrogen adsorption. The BET surface area of the bulk-PPy and PPyNWs are 35.530 $m^2\ g^{-1}$ and 117.717 $m^2\ g^{-1}$, respectively (Table S3 and Table S4). Therefore, the experimental results of nitrogen adsorption and electrochemical experiments are basically consistent.

Electrochemical stability of the prepared PPyNWs and PPyNWs/PAMAM composites was investigated by CV. Figure 3C shows that the covered area of the CV curve and oxide peak current of the redox probe ($[Fe(CN)_6]^{3/4-}$) at the PPyNWs and PPyNWs/PAMAM remain unchanged over a long time (after 50 cycles). The experimental results showed that both PPyNWs and PPyNWs/PAMAM nonocomposites had ultrahigh stability as the substrate of sensor.

Electrochemical characterization of miRNA biosensor

CV and EIS techniques were used to monitor the stepwise preparation of the miRNA biosensor using $[Fe(CN)_6]^{3/4-}$ as a redox probe (Fig. 4). As shown in Fig. 4A, after PPyNWs modified the electrode surface, the CV curve shows an significant increase in the redox currents of the Fe(III)/Fe(II) due to larger specific surface area of conducting PPyNWs. Dendrimers PAMAM as functional groups can be covalently linked to onto PPy film by an electrochemical patterning approach through amine oxidation as Miodek et al. reported previously [24]. The PAMAM/PPyNWs film supply a large amount of amine groups on the surface for further immobilization of the DNA probes. After PAMAM was were connected to PPy nanowires, the redox peak current of CV decreased significantly (curve c), which indirectly proved the successful preparation of PAMAM/PPyNWs. Subsequently, after the DNA probes and miRNA targets were successively

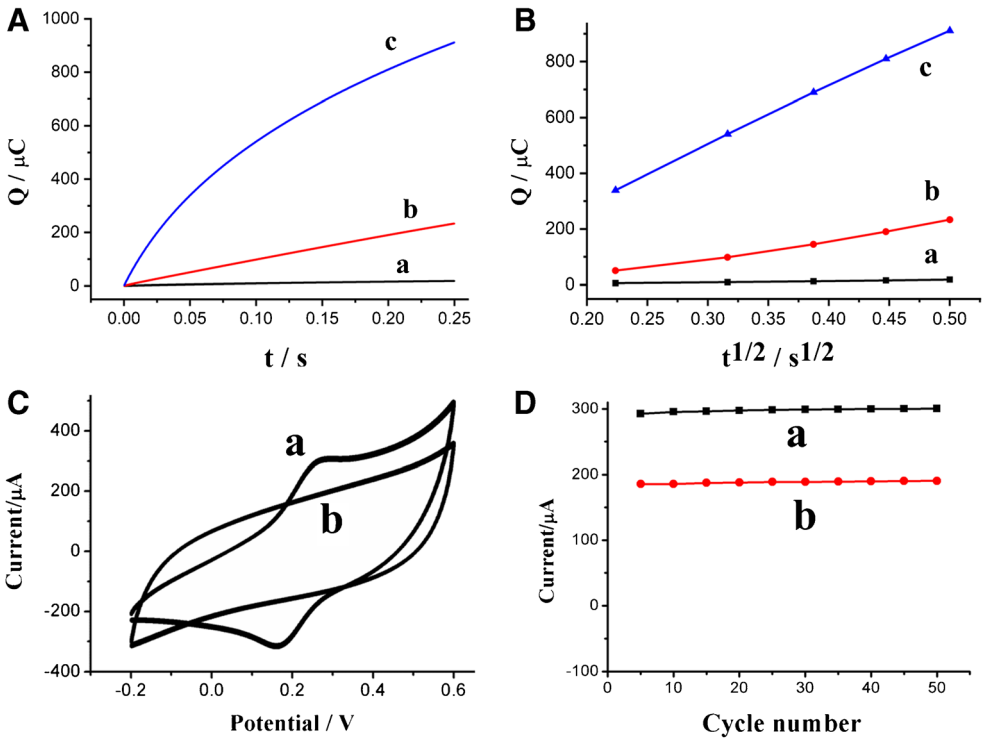

Fig. 3 (A) Chronocoulometric curves of bare GCE (a), GCE/PPy (bulk) (b) and GCE/PPyNWs (c) for the reduction of 0.2 mM $K_3Fe(CN)_6$ with 0.1 M KCl with the pulse width of 0.25 s. (B) the relationship between Q and $t^{1/2}$. (C) and (D) Electrochemical stability of the prepared PPyNWs (a) and PPyNWs/PAMAM (b) composites by CV of 50 circles in the mixed solution containing 0.1 M KCl and 5 mM $[Fe(CN)_6]^{3/4-}$

immobilized on the electrode, continuous significant decrease of CV currents was observed (curve d and e). This is because the negatively charged phosphate skeletons of both single stranded DNA probes and double stranded DNA/RNA will severely repel the negatively charged $[Fe(CN)_6]^{3-/4-}$ probe.

Nyquist impedance diagram consists of a semicircle portion at high frequencies (corresponding to charge transfer) and a linear portion at lower frequencies (corresponding to diffusion limiting process) [35]. When the standard Randles equivalent circuit is fitted (inset in Fig. 4), the semicircle diameter is equal to the charge transfer resistance (R_{CT}) of the modified electrode [36]. Figure 4B shows the step-by-step fabrication procedure of the biosensor monitored by EIS. Formation of the PPyNWs arrays caused a large decrease of the charge-transfer resistance (R_{CT}) from 280 to 90 Ω, proving an electron transfer enhancement by the conducting PPyNWs arrays. During the modification of PPyNWs arrays by PAMAM, the conductivity of PPyNWs layer was destroyed by the coupling reaction between PPy and PAMAM, and the R_{CT} increased steadily to 110 Ω. The addition of DNA probes and miRNA targets resulted in an increase in R_{CT} to 210 Ω and 535 Ω, which was due to electrostatic repulsion. The results of EIS experiments are consistent with CV results, which further confirmed the successful fabrication of the biosensor.

The condition optimization

To obtain optimal experimental conditions for miRNA detection, the effects of PAMAM loading mass, the concentration of DNA probe, the immobilization time for DNA probes and the DNA/miRNA hybridization time were investigated in detail. The results are as follows. PAMAMG dendrimers were

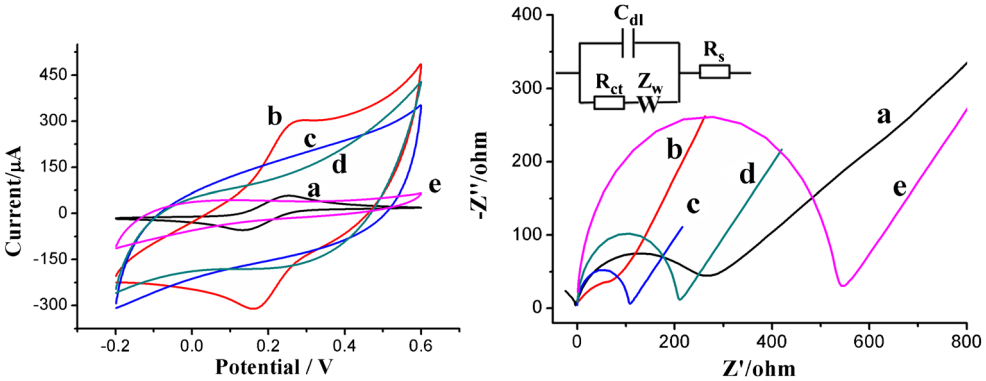

Fig. 4 (A) CV and (B) EIS tests in presence of the mixed solution of 0.1 M KCl and 5 mM $[Fe(CN)_6]^{3/4-}$ after each step of the biosensor formation (a) bare GCE, (b) GCE/PPyNWs (c) GCE/PPyNWs/PAMAM (d) GCE/PPyNWs/PAMAM/DNA (e) GCE/PPyNWs/PAMAM/DNA/RNA. Inset: the EIS equivalent circuit

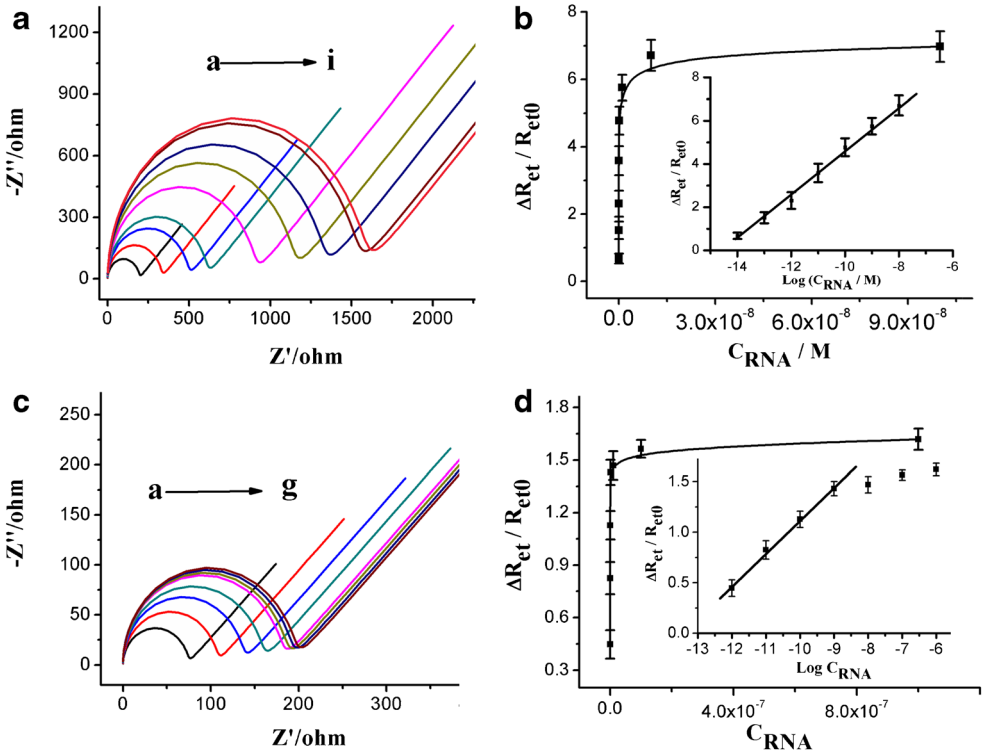

Fig. 5 EIS responses of (A) GCE/PPyNWs/PAMAM/DNA and (C) GCE/PPy/PAMAM/DNA toward different concentrations of miRNA24, curve a represents the blank solution and curves b-i (in Fig. A) correspond to miRNA24 at the concentrations from10^{-14} M to 10^{-7} M; And curves b-g (in Fig. C) correspond to miRNA24 at the concentrations from10^{-12} M to 10^{-6} M. The dynamic response ranges of (B) GCE/PPyNWs/PAMAM/DNA and (D) GCE/PPy/PAMAM/DNA upon a function of miRNA24 concentrations. Inset: corresponding calibration plot of the biosensors. Parameters of EIS measurements: the potential of 0.20 V, frequency range of 0.1 ~ 100 KHz, the applied sine wave of 5 mV

immobilized onto the PPyNWs using cyclic voltammetry by scanning the potential from 0.0 to1.1 V during 3 cycles with the scan rate of 0.10 V s^{-1}. The concentration of DNA probes and the immobilization time were selected as 10^{-6} M and 1 h, respectively. 1.0 h was chosen for the DNA/miRNA hybridization time. The detailed analysis of the experimental results is shown in the supporting materials (Fig. S3).

The sensing performance of the biosensors

EIS technique was used to detect DNA sequences because it can better study the characteristics of electrode surface and better consider the performance of the genosensor [37]. The electrochemical responses of two different biosensors (nanowires GCE/PPyNWs/PAMAM/DNA and bulk GCE/PPy/PAMAM/DNA) toward different concentrations of miRNA24 were studied in details. As shown in Fig. 5(A and C), the R_{et} changes ($\Delta R_{et}/R_{et0}$) of the two different modified biosensors decreased gradually with the increasing of miRNA24 concentrations, which demonstrated the formation of double stranded DNA/miRNA complexes. For GCE/PPyNWs/PAMAM/DNA, the R_{et} changes is linearly proportional to the logarithmic value of miRNA concentrations with a regression equation of $\Delta R_{et}/R_{et0} = 1.01$ lgC +14.73 ($R^2 = 0.996$) in the range of 10^{-14} M to 10^{-8} M. A limit of detection (LOD) of 0.34×10^{-14} M is obtained with the sensitivity of 14.30 *ss* cm^{-2}. For GCE/PPy/PAMAM/DNA, a linear regression equation of $\Delta R_{et}/R_{et0} = 0.324$ lgC +4.366 ($R^2 = 0.996$) was obtained in the linear range of 10^{-12} M to 10^{-9} M, with the limit of detection of 0.37×10^{-12} M and sensitivity of 4.58 *ss* cm^{-2}. Notably, the sensitivity of the PPyNWs-modified biosensor was more than three times than that of the bulk PPy-modified biosensor, owing to the conducting nanowire microstructure. The sensing performances of these biosensors

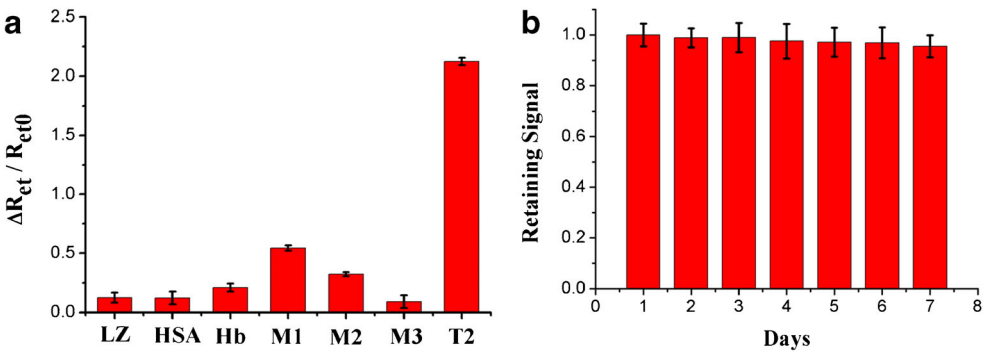

Fig. 6 (A) Responses of the biosensor to 1.0 ng mL^{-1} of LZ, HSA, Hb and 10^{-12} M of M1, M2, M3 and T2, respectively. (B) Long-time stability of the biosensor response for seven days stored in PBS (0.2 M, pH 7.4)

Table 1 Comparison of two methods for miRNA24 detection in human serum (4%, *V*/V)

Samples	miRNA measured by PCR instrument (Roche 48,011) (nM)	RSD (%)	miRNA measured by the biosensor (nM)	RSD (%)
1	35.6	4.12	37.7	5.01
2	34.2	4.02	39.4	4.67
3	38.6	5.23	40.1	4.31

were compared with that of other miRNA biosensors, as shown in Table S6. It is worth noting that the prepared biosensor showed superior sensing performances, such as wide linear range, high sensitivity and low LOD. This high performance may be due to the following reasons: (1) PPyNWs can provide excellent conductivity and the high electroactive surface area. (2) PAMAM/PPyNWs allows loading a large amount of DNA probes. The hydrophilic PAMAM/PPyNWs supply an ideal micro-environment for the DNA probes to show strong specific binding affinity toward miRNA24. These results demonstrated the potential of functionalized PPyNWs as platform for miRNA detection.

Selectivity, reproducibility and long-time stability of the biosensor

Selectivity is an important factor for practical application of the biosensor. To evaluate the specificity of the biosensor to miRNA24, the tests was performed with the selected biomolecules, such as LZ (pI = 11.0–11.2), HSA (pI = 4.7–4.90), Hb (pI = 7.07), single-based mismatch miRNA24 (M1), three-based mismatch miRNA24 (M2) and miRNA21 (M3). Figure 6 showed that the prepared biosensor showed the largest response toward miRNA24 and the negligible responses toward LZ, HAS, Hb, M1, M2 and M3 even at the high concentration. The results proved the excellent selectivity of the biosensor to miRNA24.

To test the reproducibility of the biosensor, miRNA24 at 10^{-12} M were detected by six electrodes. The relative standard deviation (RSD) was 5.1%. The same biosensor was repeated six times for the same concentration of miRNA24 (10^{-12} M), and the RSD was calculated to be 3.7%. Moreover, long-term stability of the biosensor was also tested by continuously recording the biosensor signal responses for seven days. Figure 6B showed that the biosensor kept 95% of its first day signal after seven days. The results showed good stability of the PPyNWs/PAMAM hybrid-based biosensor.

The miRNA detection in human serum samples

To investigate GCE/PPy/PAMAM/DNA for clinical detection, three human serum samples (4%, *V*/V) have been tested in parallel using both PCR and the new prepared biosensor. These samples were detected with fluorescence quantitative PCR instrument (Roche 48,011) and then analyzed with the biosensor. As shown in Table 1, these results of the biosensor and PCR are very close.

Conclusions

PPyNWs/PAMAM composite with nanowires morphology, outstanding stability and good conductivity was successfully prepared by an electrochemical patterning. Firstly, PPyNWs was electrodeposited onto the electrode surface by template free and show excellent electrical stability and good conductivity. Then the modification of PPyNWs with PAMAM onto the conducting polymer nanowires can be achieved by electrochemical oxidation of the amine groups of PAMAM. GCE/PPyNWs/PAMAM has a higher active specific surface area than GCE/PPY, which allows more DNA probes to be attached to the modified electrodes, so GCE/PPyNWs/PAMAM has better sensing performance. There are some limitations in this work. For example, the antifouling performance of the modified electrodes has not been discussed. It is also expected that the functionalized conducting polymer nanowires can supply a substrate for the preparation of other electrochemical biosensors.

Supplementary Information The online version contains supplementary material available at https://doi.org/10.1007/s00604-021-04824-y.

Acknowledgments This research was supported by the National Natural Science Foundation of China (21705088), Major Agricultural Application Technology Innovation Projects in Shandong Province China (SD2019NJ001-2), China Shandong Science and Technology Program (J14LB14), the Qingdao Agricultural University High-level Talent Project (663/1117025).

Declarations

Conflict of interest The authors declare that they have no known competing financial interests or personal relationships that could have appeared to influence the work reported in this paper.

References

1. Mori M, Triboulet R, Mohseni M, Schlegelmilch K, Shrestha K, Camargo FD, Gregory RI (2014) Hippo signaling regulates microprocessor and links cell density-dependent miRNA biogenesis to cancer. Cell 156(5):893–906
2. Borghei YS, Hosseini M, Ganjali MR (2017) Fluorescence based turn-on strategy for determination of microRNA-155 using DNA-templated copper nanoclusters. Microchim Acta 184(8):2671–2677
3. Bharti A, Agnihotri N, Prabhakar N (2019) A voltammetric hybridization assay for microRNA-21 using carboxylated graphene oxide decorated with gold-platinum bimetallic nanoparticles. Microchim Acta 186(3):185
4. Jing P, Tao H, Yulian S, Yawen L, Qianqian C, Qiong W, Hao T (2018) An organic electrochemical transistor for determination of microRNA21 using gold nanoparticles and a capture DNA probe. Microchim Acta 185(9):408
5. Duan R, Zuo X, Wang S, Quan X, Chen D, Chen Z, Lei J, Fan C, Fan X (2013) Lab in a tube: ultrasensitive detection of MicroRNAs at the single-cell level and in breast Cancer patients using quadratic isothermal amplification. J Am Chem Soc 135(12):4604–4607
6. Jin Z, Geißler D, Qiu X, Wegner KD, Hildebrandt N (2015) A rapid, amplification-free, and sensitive diagnostic assay for single-step multiplexed fluorescence detection of MicroRNA. Angew Chem Int Ed 54:10024–10029
7. Tian L, Qian K, Qi J, Liu Q, Yao C, Song W, Wang Y (2018) Gold nanoparticles superlattices assembly for electrochemical biosensor detection of microRNA-21. Biosens Bioelectron 99:564–570
8. Lusi EA, Passamano M, Guarascio P, Scarpa A, Schiavo L (2009) Innovative electrochemical approach for an early detection of microRNAs. Anal Chem 81(7):2819–2822
9. Kangkamano T, Numnuam A, Limbut W, Kanatharana P, Vilaivan T, Thavarungkul P (2017) Pyrrolidinyl PNA polypyrrole/silver nanofoam electrode as a novel label-free electrochemical miRNA-21 biosensor. Biosens Bioelectron 102:217–225
10. Lei W, He P, Wang Y, Zhang S, Dong F, Liu H (2014) Soft template interfacial growth of novel ultralong polypyrrole nanowires for electrochemical energy storage. Electrochim Acta 132:112–117
11. Rajesh, Ahuja T, Kumar D (2009) Recent progress in the development of nano-structured conducting polymers/nanocomposites for sensor applications. Sensors Actuators B Chem 136(1):275–286
12. Thi L, Tran TXC, Quan DP, Thanh PD, Quan TVV, Chinh HD, Tuan MA (2015) In-Channel-grown Polypyrrole nanowire for the detection of DNA hybridization in an electrochemical microfluidic biosensor. J Nanomater 2015:2
13. Ramanathan K, Bangar MA, Yun M, Chen W, Myung NV (2004) Individually addressable conducting polymer nanowires Array. Nano Lett 4(7):1237–1239
14. Debiemme-Chouvy C, Fakhry A, Pillier FO (2018) Electrosynthesis of polypyrrole nano/micro structures using an electrogenerated oriented polypyrrole nanowire array as framework. Electrochim Acta 268:66–72
15. Huang Z, Song Y, Xu X, Liu X (2015) Ordered Polypyrrole nanowire arrays grown on a carbon cloth substrate for a high-performance Pseudocapacitor electrode. ACS Appl Mater Interfaces 7(45):25506–25513
16. Khoder R, Korri-Youssoufi H E-DNA biosensors of M. tuberculosis based on nanostructured polypyrrole. Mater Sci Eng C 108: 110371
17. Ahmad L, Salmon L, Korri-Youssoufi H (2019) Electrochemical detection of the human cancer biomarker 'autocrine motility factor-phosphoglucose isomerase' based on a biosensor formed with a monosaccharidic inhibitor. Sensors Actuators B Chem 299:126933
18. Wang J, Hui N (2019) Electrochemical functionalization of polypyrrole nanowires for the development of ultrasensitive biosensors for detecting microRNA. Sensors Actuators B Chem B281:478–485
19. Xia Z, Wang S, Jiang L, Sun H, Sun G (2014) Controllable synthesis of vertically aligned polypyrrole nanowires as advanced electrode support for fuel cells. J Power Sources 256(Jun.15): 125–132
20. Duc T, Pham N, Minh H, Nguyen H, Hai M (2014) Highly sensitive DNA sensor based on polypyrrole nanowire. Appl Surf Sci 309: 285–289
21. Zhu N, Gao H, Xu Q, Lin Y, Su L, Mao L (2010) Sensitive impedimetric DNA biosensor with poly(amidoamine) dendrimer covalently attached onto carbon nanotube electronic transducers as the tether for surface confinement of probe DNA. Biosens Bioelectron 25(6):1498–1503
22. Tsukruk VV, Rinderspacher F, Bliznyuk VN (1997) Self-assembled multilayer films from Dendrimers. Langmuir 13(8): 2171–2176
23. Miodek A, Castillo G, Hianik T, Korriyoussoufi H (2013) Electrochemical Aptasensor of human cellular prion based on multiwalled carbon nanotubes modified with Dendrimers: a platform for connecting redox markers and Aptamers. Anal Chem 85(16):7704–7712
24. Miodek A, Mejriomrani N, Khoder R, Korriyoussoufi H (2016) Electrochemical functionalization of polypyrrole through amine oxidation of poly(amidoamine) dendrimers: application to DNA biosensor. Talanta 154:446–454
25. Li Q, Yu C, Gao R, Xia C, Yuan G, Li Y, Zhao Y, Chen Q, He J (2016) A novel DNA biosensor integrated with Polypyrrole/streptavidin and au-PAMAM-CP bionanocomposite probes to detect the rs4839469 locus of the vangl1 gene for dysontogenesis prediction. Biosens Bioelectron 80:674–681
26. Hui N, Sun X, Niu S, Luo X (2017) PEGylated Polyaniline Nanofibers: antifouling and conducting biomaterial for electrochemical DNA sensing. ACS Appl Mater Interfaces 9(3):2914–2923
27. Lassalle N, Vieil E, Correia JP, Abrantes LM (2001) Study of DNA hybridization by photocurrent spectroscopy. Synth Met 119(1–3): 407–408
28. Xia Z, Wang S, Li Y, Jiang L, Sun H, Zhu S, Su DS, Sun G (2013) Vertically oriented polypyrrole nanowire arrays on Pd-plated Nafion® membrane and its application in direct methanol fuel cells. J Mater Chem 1(3):491–494
29. Ghanem MA, Chretien J, Pinczewska A, Kilburn JD, Bartlett PN (2008) Covalent modification of glassy carbon surface with organic redox probes through diamine linkers using electrochemical and solid-phase synthesis methodologies. J Mater Chem 18(41):4917–4927
30. Chrétien JM, Ghanem MA, Bartlett PN, Kilburn JD (2010) Covalent tethering of organic functionality to the surface of glassy carbon electrodes by using electrochemical and solid-phase synthesis methodologies. Chem Eur J 14(8):2548–2556
31. Zhang L, Jiang X, Wang E, Dong S (2006) Attachment of gold nanoparticles to glassy carbon electrode and its application for the direct electrochemistry and electrocatalytic behavior of hemoglobin. Biosens Bioelectron 21:337–345
32. Barbier B (1990) Electrochemical bonding of amines to carbon Fiber surfaces toward improved carbon-epoxy composites. J Electrochem Soc 137(6):1757–1764
33. Wenzel RN (1936) Resistance of solid surfaces to wetting by water. Ind Eng Chem 28(8):988–994

34. Csiszar M, Szucs A, Tolgyesi M, Mechler A, Nagy JB, Novak M (2001) Electrochemical reactions of cytochrome c on electrodes modified by fullerene films. J Electroanal Chem 497(1):69–74
35. Xu M, Luo X, Davis JJ (2013) The label free picomolar detection of insulin in blood serum. Biosens Bioelectron 39:21–25
36. Guo XF, Kulkarni A, Doepke A, Halsall HB, Iyer S, Heineman WR (2012) Carbohydrate-based label-free detection of Escherichia coli ORN 178 using electrochemical impedance spectroscopy. Anal Chem 84:241–246
37. Migliorini FL, Sanfelice RC, Mercante LA, Andre RS, Mattoso LHC, Correa DS (2018) Urea impedimetric biosensing using electrospun nanofibers modified with zinc oxide nanoparticles. Appl Surf Sci 443:18–23